Internship Research Project Report

Yu Du
yu.du2@ucdconnect.ie
github.com/Godot008/Internshi_Project

September 3, 2025

Abstract

The PD-1 immune checkpoint pathway plays a pivotal role in regulating T cell activation and maintaining immune homeostasis. A deeper understanding of the dynamic proteomic changes following PD-1 engagement is essential for uncovering potential biomarkers and therapeutic targets, as well as elucidating mechanisms of immune checkpoint inhibitor (ICI) resistance. In this project, I performed quantitative proteomic profiling of PD-1 reporter and control conditions at three time points (5 minutes, 20 minutes, and 4 hours) after TCR stimulation. Raw abundance data were processed through coverage and abundance filtering, log2 transformation, and batch effect correction using ComBat. Differential expression analysis was followed by hierarchical clustering, pathway enrichment, and STRING protein-protein interaction (PPI) network visualization. In this project, I performed quantitative proteomic profiling of PD-1 reporter and control conditions at three time points (5 minutes, 20 minutes, and 4 hours) after TCR stimulation. Raw abundance data were processed through coverage and abundance filtering, log2 transformation, and batch effect correction using ComBat. Differential expression analysis was followed by hierarchical clustering, pathway enrichment, and STRING protein-protein interaction (PPI) network visualization. A total of 16 significantly regulated proteins were identified. Time-resolved clustering revealed distinct expression modules, with one cluster enriched in ribosomal and metabolic processes (e.g., RPL22, CS, PLG), while another cluster highlighted immune-related pathways and chromatin-associated proteins (e.g., HBA2, H2AC21). Enrichment analyses demonstrated associations with pathways such as ribosome function, viral defense, necroptosis, and complement cascades, with FDR correction enhancing the robustness of biologically meaningful modules. STRING PPI analysis further identified key hub proteins (e.g., RPL22, HBA2, H2AC21) that may serve as central regulators in PD-1-mediated immune modulation. These results provide proteomic-level evidence that PD-1 activation reshapes TCR signaling in a temporally dynamic manner. By identifying functionally enriched protein clusters and network hubs, this work advances our understanding of ICI mechanisms, offers new insights into resistance development, and highlights candidate proteins as potential therapeutic targets.

1 Introduction

In recent years, cancer immunotherapy has made remarkable advances, aiming to enhance the immune system's ability to recognize and eliminate tumor cells, thereby improving the specificity and durability of anticancer responses (Han et al., 2020). Among immune checkpoints, programmed cell death protein 1 (PD-1) is a pivotal inhibitory receptor and a major target of immune checkpoint inhibitors (ICIs). Binding of PD-1 to its ligands (PD-L1 and PD-L2) suppresses T cell receptor (TCR)-mediated signaling and modulates multiple key pathways, ultimately impairing T cell activation. Tumor cells often exploit this mechanism to evade immune surveillance (Mizuno et al., 2019; Chen et al., 2025).

While transcriptomic studies have revealed aspects of PD-1-related signaling, they primarily capture transcriptional regulation and cannot directly reflect functional effectors or post-transcriptional regulation. Proteomics, in contrast, directly measures the functional molecular landscape, providing quantitative information on protein abundance, post-translational modifications, and dynamic signaling processes. This makes proteomic profiling particularly valuable for elucidating PD-1 signaling mechanisms.

In this internship research project, I utilized quantitative whole-proteome data[1] of the Jurkat T cell line[2] acquired via mass spectrometry using the MaxLFQ algorithm, under PD-1 stimulation at multiple time points (5 min, 20 min, 4 h). I systematically investigated the temporal dynamics of protein expression, including:

1. Differential protein identification with time-integrated analysis;
2. Clustering-based detection of early- and late-response patterns;
3. Gene Ontology (GO) and Kyoto Encyclopedia of Genes and Genomes (KEGG) enrichment analyses to reveal associated biological processes and pathways;
4. Construction of protein-protein interaction (PPI) networks to identify potential key regulators.

This work aims to elucidate the effects of PD-1 activation on TCR signaling and downstream immune regulation, providing proteomic-level evidence to advance our understanding of ICI mechanisms, resistance development, and the discovery of novel therapeutic targets.

2 Methods

2.1 Data Sources and Data Pre-Processing

The proteomic dataset used in this project was obtained from quantitative mass spectrometry (MaxLFQ method) of Jurkat T cells, including PD-1 reporter and control groups at three time points: 5 min, 20 min, and 4 h.

[1] I have stored the original data, generated intermediate data and result data on my Google Drive at UCD (https://drive.google.com/drive/folders/1-tbezxn0ImQxPkNMIwaoOBjEl7V8tOTd?usp=share_link) for reference.

[2] This cell line is widely used as an in vitro model for T cell signaling studies due to its high reproducibility.

Pre-processing steps were as follows:

1. Data formatting to retain only relative abundance values and ensure compliance with first normal form (1NF).
2. **Coverage filtering:** removing proteins with >50% missing values.
3. **Abundance filtering:** removing proteins with low total abundance across all samples, based on the initial dataset size (6,270 proteins) and observed abundance distribution.
4. **Batch effect correction:** batch information was extracted from sample IDs (ProtA-ProtD) using regular expressions and recorded in the metadata table; applying `scanpy.pp.combat()` on log2-transformed data, using batch (A-D) as the primary variable and experimental condition and time point as covariates; PCA was performed before and after batch correction, and PC1-PC2 scatter plots were generated to evaluate the removal of batch effects while retaining biological separation.
5. **Outlier handling:** applying winsorization (upper/lower bound trimming) or removing proteins with Z-scores > 5 for specific analyses;
6. **Standardization:** prior to heatmap plotting, applying row-wise Z-score standardization (`standard_scale=1`) and selecting the top 30 most significant proteins for visualization.

2.2 Differential Expression Analysis

To compare protein expression differences between the PD-1 reporter group and the control group at each time point, Welch's t-test was applied to calculate the statistical significance (p-values) for each protein, followed by false discovery rate (FDR) correction using the Benjamini-Hochberg method. Both unadjusted results ($p < 0.05$) and FDR-adjusted results (FDR < 0.1) were retained to allow for direct comparison of findings under different significance criteria in the Results section. The thresholds for log2 fold change (log2FC) were set as follows: absolute log2FC > 1.0 for unadjusted results and > 0.5 for FDR-adjusted results, where log2FC was defined as the log2-transformed difference between group mean abundances.

Following the identification of differentially expressed proteins, they were further classified into upregulated and downregulated (negatively regulated) proteins based on the sign of log2FC, thereby clarifying the direction of expression change under each condition. To obtain a comprehensive set of differentially expressed proteins, results from the three time points were combined, and any protein significant at least at one time point was retained to capture time-specific changes and avoid omitting potentially important candidates.

2.3 Functional and Pathway Enrichment Analysis

For each protein cluster, pathway enrichment analysis was performed using the `gseapy.enrichr()` function against Reactome, Gene Ontology (GO), and Kyoto Encyclopedia of Genes and Genomes (KEGG) databases. This method employs Fisher's exact test to calculate enrichment significance.

2.4 Protein-protein interaction (PPI) network

Gene sets of significant proteins were queried against the STRING database (v11.5) API for human proteins (taxon ID: 9606) with a minimum interaction confidence score of 0.4. If no interactions were found, the threshold was automatically lowered to 0.15, and first-shell neighbors could optionally be added to expand the network. Isolated nodes were retained in the visualization to ensure complete representation of the input proteins, facilitating comprehensive interpretation of network structure and potential regulatory relationships.

2.5 Clustering and Visualization

Hierarchical clustering was performed on standardized expression values of significant proteins. The optimal number of clusters was determined using dendrogram inspection combined with biological interpretation. Heatmap clustering was used to identify early- and late-response protein expression patterns.

3 Results

3.1 Data Sources and Data Pre-Processing

After applying combined coverage and abundance filtering, the number of proteins was reduced from the initial 6,270 to 866 (Figure 1). As shown in the abundance distribution histograms, the raw data exhibited a strong bias with most proteins concentrated in the low-abundance range, whereas after filtering, low-abundance noise was effectively removed and the overall distribution became more balanced, thereby improving the robustness of downstream analyses (Figure 1a vs. 1b).

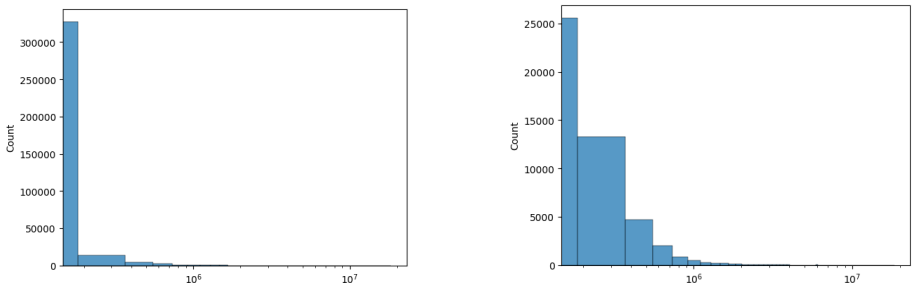

(a) Original abundance distribution.

(b) Filtered abundance distribution.

Figure 1: Comparison of protein abundance distribution before and after filtering.

Subsequently, batch correction was performed using the ComBat method. Before correction, PCA revealed a clear separation of samples driven by batch effects, indicating that batch variation had a substantial influence on the data structure. After correction, the separation by batch was greatly reduced and samples from different batches were well mixed, while the biological separation trend remained preserved. This demonstrates that batch correction effectively removed non-biological variation (Figure 2, left vs. right).

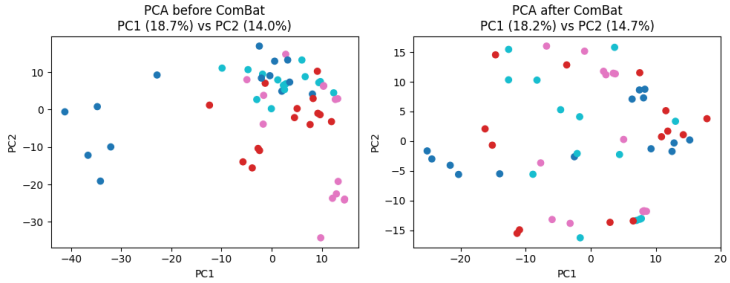

Figure 2: Comparison of PCA test results before and after batch correction.

3.2 Differential Expression Analysis

In the differential expression analysis, I compared the PD-1 activated group with the control group at three time points: 5 minutes, 20 minutes, and 4 hours (Table 1). At the raw p-value threshold, several proteins were found to be significantly different at 5 minutes, including HNRNPLL, CACTIN, HBD, and SORL1. After FDR adjustment, the number of significant proteins was reduced, but notable hits such as PLG, HBA2, EWSR1, and H2AC21 remained significant. At 20 minutes, BLTP3A and LNPK showed significance under raw p-values but did not pass FDR correction. In contrast, at 4 hours, a larger set of stable differentially expressed proteins was identified. For example, RPL22 was significant under both raw and adjusted criteria, while proteins such as CS, BTF3, EIF6, RPL18A, and NUDT5 emerged as significant only after FDR correction.

Table 1: PD-1 differential expression analysis results at multiple time points.

5 minutes

Gene	log2FC	p_value	p_fdr	significant	significant_fdr
Raw results					
HBD	1.2808	0.0276	0.3023	True	False
H2BC20P	1.0544	0.0091	0.1727	True	False
CACTIN	-1.7535	0.0345	0.3166	True	False
HNRNPLL	1.1090	0.0461	0.3380	True	False
SORL1	8.5232	0.0159	0.2202	True	False
FDR-adjusted results					
PLG	0.7115	3.21e-07	0.000275	False	True
HBA2	0.7566	2.32e-03	0.090330	False	True
EWSR1	0.6049	1.98e-04	0.028381	False	True
H2AC21	0.5224	4.56e-04	0.043509	False	True

20 minutes

Gene	log2FC	p_value	p_fdr	significant	significant_fdr
Raw results					
BLTP3A	8.5822	0.0428	0.9992	True	False
LNPK	13.2795	0.0003	0.2209	True	False
FDR-adjusted results					
— None —					

4 hours

Gene	log2FC	p_value	p_fdr	significant	significant_fdr
Raw results					
RPLP1	-1.1547	0.0304	0.1290	True	False
RPL22	-1.0164	0.0032	0.0841	True	True
PPIA	-1.3549	0.0322	0.1302	True	False
HNRNPLL	-1.2272	0.0341	0.1304	True	False
FDR-adjusted results					
CS	-0.6801	0.0091	0.0995	False	True
BTF3	-0.6782	0.0065	0.0982	False	True
RPL22	-1.0164	0.0032	0.0841	True	True
EIF6	-0.5815	0.0061	0.0974	False	True
RPL18A	-0.7351	0.0011	0.0797	False	True
NUDT5	-0.5758	0.0094	0.0995	False	True

These results suggest that PD-1 activation triggers modest early molecular changes

at 5 minutes (Figure 3a), most of which do not remain significant after multiple testing correction. At 20 minutes (3b), the response appears transient and weak. However, by 4 hours (Figure 3c), a more robust set of downregulated proteins emerges, indicating that the inhibitory effects of PD-1 stimulation become more pronounced over time. The volcano plots (Figure 3) provide a visual comparison of differential expression patterns under both raw p-value and FDR-adjusted criteria across all time points.

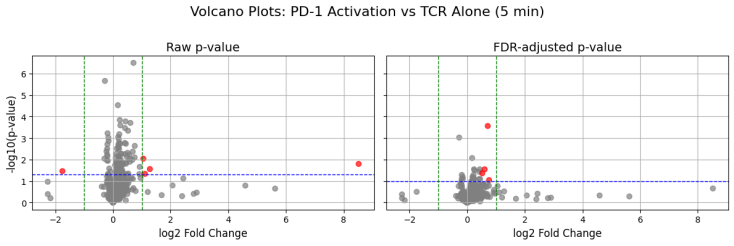

(a) 5 minutes.

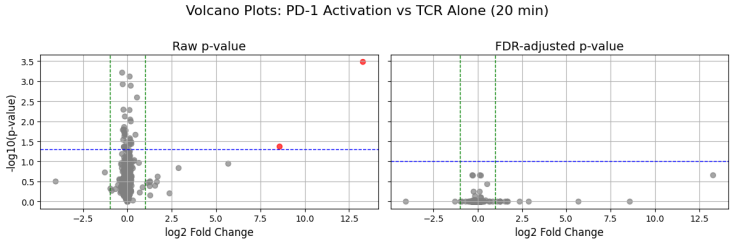

(b) 20 minutes.

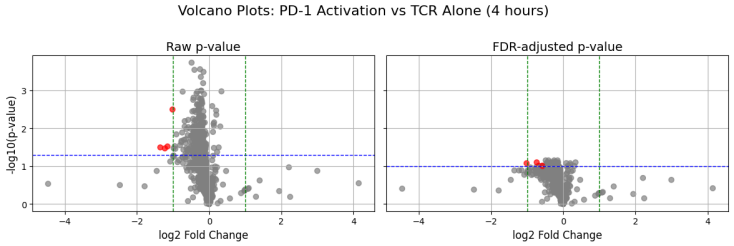

(c) 4 hours.

Figure 3: Volcano plot analysis results of PD-1 differential expression at multiple time points.

3.3 Functional and Pathway Enrichment Analysis

3.3.1 Gene Enrichment Analysis

Gene set enrichment analysis revealed distinct temporal dynamics following PD-1 activation.

At 5 minutes, before FDR correction, differentially expressed genes (DEGs) were mainly enriched in GO biological processes related to protein transport, receptor recycling, and metabolic regulation, such as protein retention in the Golgi apparatus, regulation of protein localization, ER-to-Golgi vesicle-mediated transport, and endocytic recycling. Key driver genes included SORL1 and CACTIN. After FDR correction, the number of significant terms decreased, but enrichment remained evident in pathways associated with complement and coagulation cascades, fibrinolysis, regulation of blood coagulation, and immune-related processes (e.g., systemic lupus erythematosus, influenza A infection, cytokine signaling), involving genes such as PLG, HBA2, EWSR1, and H2AC21. These results suggest that PD-1 activation exerts early effects on immune and coagulation-related signaling pathways.

Table 2: PD-1 differential expression enrichment analysis at 5 minutes (Raw results, top 20).

Gene set	Term	Overlap	P-value	Adj. P-value	Genes
GO Biological Process 2021	protein retention in Golgi apparatus (GO:0045053)	1/5	0.001249	0.021099	SORL1
GO Biological Process 2021	negative regulation of triglyceride metabolic process	1/6	0.001499	0.021099	SORL1
GO Biological Process 2021	regulation of adipose tissue development (GO:1904177)	1/6	0.001499	0.021099	SORL1
GO Biological Process 2021	positive regulation of protein localization to membrane (GO:1905744)	1/8	0.001999	0.021099	SORL1
GO Biological Process 2021	positive regulation of endocytic recycling (GO:2001134)	1/8	0.001999	0.021099	SORL1
GO Biological Process 2021	regulation of protein localization to early endosome (GO:2000643)	1/8	0.001999	0.021099	SORL1
GO Biological Process 2021	regulation of aspartic-type endopeptidase activity	1/9	0.002248	0.021099	SORL1
GO Biological Process 2021	regulation of ER to Golgi vesicle-mediated transport	1/9	0.002248	0.021099	SORL1
GO Biological Process 2021	negative regulation of inclusion body assembly	1/10	0.002498	0.021099	SORL1
GO Biological Process 2021	negative regulation of interferon-beta production	1/10	0.002498	0.021099	CACTIN
GO Biological Process 2021	negative regulation of lipopolysaccharide-mediated signaling	1/10	0.002498	0.021099	CACTIN
GO Biological Process 2021	receptor recycling (GO:0001881)	1/10	0.002498	0.021099	SORL1
GO Biological Process 2021	regulation of tau-protein kinase activity (GO:2000463)	1/10	0.002498	0.021099	SORL1
GO Biological Process 2021	positive regulation of cytoplasmic transport (GO:1903829)	1/11	0.002747	0.021099	SORL1
GO Biological Process 2021	regulation of endocytic recycling (GO:2001135)	1/11	0.002747	0.021099	SORL1
GO Biological Process 2021	regulation of triglyceride catabolic process (GO:0010898)	1/12	0.002997	0.021099	SORL1
GO Biological Process 2021	positive regulation of insulin receptor signaling pathway (GO:0046628)	1/13	0.003246	0.021099	SORL1
GO Biological Process 2021	positive regulation of protein exit from endoplasmic reticulum (GO:1900100)	1/13	0.003246	0.021099	SORL1
GO Biological Process 2021	regulation of protein exit from endoplasmic reticulum (GO:1900101)	1/13	0.003246	0.021099	SORL1

Table 3: PD-1 differential expression enrichment analysis at 5 minutes (FDR-adjusted results, top 20).

Gene set	Term	Overlap	P-value	Adj. P-value	Genes
KEGG 2021 Human	African trypanosomiasis	1/37	0.007380	0.041638	HBA2
KEGG 2021 Human	Malaria	1/50	0.009963	0.041638	HBA2
KEGG 2021 Human	Complement and coagulation cascades	1/85	0.016893	0.041638	PLG
KEGG 2021 Human	Staphylococcus aureus infection	1/95	0.018866	0.041638	PLG
KEGG 2021 Human	Systemic lupus erythematosus	1/135	0.026730	0.041638	H2AC21
KEGG 2021 Human	Necroptosis	1/159	0.031425	0.041638	H2AC21
KEGG 2021 Human	Influenza A	1/172	0.033961	0.041638	PLG
KEGG 2021 Human	Alcoholism	1/186	0.036687	0.041638	H2AC21
KEGG 2021 Human	Neutrophil extracellular trap formation	1/189	0.037270	0.041638	H2AC21
KEGG 2021 Human	Transcriptional misregulation in cancer	1/192	0.037853	0.041638	EWSR1
KEGG 2021 Human	Neuroactive ligand-receptor interaction	1/341	0.066480	0.066480	PLG
GO Biological Process 2021	negative regulation of fibrinolysis (GO:0051918)	1/9	0.001799	0.013914	PLG
GO Biological Process 2021	negative regulation of cell-cell adhesion mediated by cadherin	1/10	0.001999	0.013914	PLG
GO Biological Process 2021	regulation of fibrinolysis (GO:0051917)	1/13	0.002598	0.013914	PLG
GO Biological Process 2021	fibrinolysis (GO:0042730)	1/15	0.002997	0.013914	PLG
GO Biological Process 2021	positive regulation of blood coagulation (GO:0030194)	1/17	0.003396	0.013914	PLG
GO Biological Process 2021	regulation of cell-cell adhesion mediated by cadherin	1/19	0.003795	0.013914	PLG
GO Biological Process 2021	negative regulation of blood coagulation (GO:0030195)	1/40	0.007977	0.018860	PLG
GO Biological Process 2021	negative regulation of cell-substrate adhesion (GO:0031589)	1/40	0.007977	0.018860	PLG
GO Biological Process 2021	negative regulation of cell-cell adhesion (GO:0022408)	1/41	0.008175	0.018860	PLG

At 20 minutes, uncorrected results indicated enrichment of processes related to

endoplasmic reticulum organization and organelle maintenance, driven primarily by LNPK. However, no significant enrichment was detected after FDR correction, suggesting that PD-1 signaling at this stage may represent a transitional phase, with insufficient molecular perturbations to yield robust enrichment results.

Table 4: PD-1 differential expression enrichment analysis at 20 minutes (Raw results, top 20).

Gene set	Term	Overlap	P-value	Adj. P-value	Genes
GO Biological Process 2021	regulation of endoplasmic reticulum tubular network organization	1/6	0.000600	0.003999	LNPK
GO Biological Process 2021	cellular component maintenance (GO:0043954)	1/13	0.001300	0.003999	LNPK
GO Biological Process 2021	endoplasmic reticulum tubular network organization (GO:0071786)	1/15	0.001499	0.003999	LNPK
GO Biological Process 2021	limb development (GO:0060173)	1/29	0.002898	0.005276	LNPK
GO Biological Process 2021	positive regulation of organelle organization (GO:0010638)	1/33	0.003297	0.005276	LNPK
GO Biological Process 2021	endoplasmic reticulum organization (GO:0007029)	1/73	0.007287	0.009716	LNPK
GO Biological Process 2021	endomembrane system organization (GO:0010256)	1/199	0.019801	0.022630	LNPK
GO Biological Process 2021	organelle organization (GO:0006996)	1/420	0.041560	0.041560	LNPK

At 4 hours, enrichment was dominated by processes associated with protein synthesis and ribosome function. Prior to FDR correction, DEGs were significantly enriched in pathways such as ribosome, cytoplasmic translation, SRP-dependent protein targeting, rRNA metabolism, and mRNA degradation, mainly involving RPLP1, RPL22, and PPIA. After FDR correction, these signals remained robust, with additional enrichment in ribosome biogenesis, rRNA processing, protein translation, and metabolic pathways including the TCA cycle and purine metabolism, involving genes such as EIF6 and NUDT5. These findings indicate that prolonged PD-1 activation strongly suppresses ribosome biogenesis, protein translation, and energy metabolism, consistent with its role in T cell functional inhibition.

Table 5: PD-1 differential expression enrichment analysis at 4 hours (Raw results, top 20).

Gene set	Term	Overlap	P-value	Adj. P-value	Genes
KEGG 2021 Human	Ribosome	2/158	0.000368	0.001105	RPLP1; RPL22
KEGG 2021 Human	Coronavirus disease	2/232	0.000792	0.001187	RPLP1; RPL22
KEGG 2021 Human	Necroptosis	1/159	0.031425	0.031425	PPIA
GO Biological Process 2021	SRP-dependent cotranslational protein targeting to membrane	2/90	0.000119	0.003128	RPLP1; RPL22
GO Biological Process 2021	cytoplasmic translation (GO:0002181)	2/93	0.000128	0.003128	RPLP1; RPL22
GO Biological Process 2021	cotranslational protein targeting to membrane (GO:0006613)	2/94	0.000130	0.003128	RPLP1; RPL22
GO Biological Process 2021	protein targeting to ER (GO:0045047)	2/103	0.000157	0.003128	RPLP1; RPL22
GO Biological Process 2021	nuclear-transcribed mRNA catabolic process, nonsense-mediated decay (GO:0000184)	2/113	0.000188	0.003128	RPLP1; RPL22
GO Biological Process 2021	rRNA metabolic process (GO:0016072)	2/162	0.000387	0.004070	RPLP1; RPL22
GO Biological Process 2021	peptide biosynthetic process (GO:0043043)	2/162	0.000387	0.004070	RPLP1; RPL22
GO Biological Process 2021	nuclear-transcribed mRNA catabolic process (GO:0000956)	2/171	0.000431	0.004070	RPLP1; RPL22
GO Biological Process 2021	rRNA processing (GO:0006364)	2/173	0.000441	0.004070	RPLP1; RPL22
GO Biological Process 2021	ribosome biogenesis (GO:0042254)	2/192	0.000543	0.004490	RPLP1; RPL22
GO Biological Process 2021	ncRNA processing (GO:0034470)	2/201	0.000595	0.004490	RPLP1; RPL22
GO Biological Process 2021	translation (GO:0006412)	2/214	0.000674	0.004663	RPLP1; RPL22
GO Biological Process 2021	negative regulation of protein polyubiquitination (GO:0031398)	1/5	0.001000	0.006383	PPIA
GO Biological Process 2021	negative regulation of stress-activated protein kinase signaling cascade (GO:0032874)	1/7	0.001399	0.007808	PPIA
GO Biological Process 2021	cellular macromolecule biosynthetic process (GO:0034645)	2/314	0.001444	0.007808	RPLP1; RPL22
GO Biological Process 2021	fusion of virus membrane with host plasma membrane (GO:0019064)	1/8	0.001599	0.007808	PPIA
GO Biological Process 2021	membrane fusion involved in viral entry into host cell (GO:0039654)	1/8	0.001599	0.007808	PPIA

Table 6: PD-1 differential expression enrichment analysis at 4 hours (FDR-adjusted results, top 20).

Gene set	Term	Overlap	P-value	Adj. P-value	Genes
KEGG 2021 Human	Ribosome	2/158	0.000911	0.005466	RPL18A; RPL22
KEGG 2021 Human	Coronavirus disease	2/232	0.001949	0.005847	RPL18A; RPL22
KEGG 2021 Human	Glyoxylate and dicarboxylate metabolism	1/30	0.008967	0.013451	CS
KEGG 2021 Human	Citrate cycle (TCA cycle)	1/30	0.008967	0.013451	CS
KEGG 2021 Human	Ribosome biogenesis in eukaryotes	1/108	0.031969	0.038086	EIF6
KEGG 2021 Human	Purine metabolism	1/129	0.038086	0.038086	NUDT5
GO Biological Process 2021	rRNA processing (GO:0006364)	3/173	0.000012	0.000529	EIF6; RPL18A; RPL22
GO Biological Process 2021	ribosome biogenesis (GO:0042254)	3/192	0.000017	0.000529	EIF6; RPL18A; RPL22
GO Biological Process 2021	SRP-dependent cotranslational protein targeting to membrane	2/90	0.000297	0.004015	RPL18A; RPL22
GO Biological Process 2021	cytoplasmic translation (GO:0002181)	2/93	0.000317	0.004015	RPL18A; RPL22
GO Biological Process 2021	cotranslational protein targeting to membrane (GO:0006613)	2/94	0.000324	0.004015	RPL18A; RPL22
GO Biological Process 2021	protein targeting to ER (GO:0045047)	2/103	0.000389	0.004017	RPL18A; RPL22
GO Biological Process 2021	nuclear-transcribed mRNA catabolic process, nonsense-mediated decay (GO:0000184)	2/113	0.000468	0.004142	RPL18A; RPL22
GO Biological Process 2021	rRNA metabolic process (GO:0016072)	2/162	0.000957	0.006197	RPL18A; RPL22
GO Biological Process 2021	peptide biosynthetic process (GO:0043043)	2/162	0.000957	0.006197	RPL18A; RPL22
GO Biological Process 2021	nuclear-transcribed mRNA catabolic process (GO:0000956)	2/171	0.001066	0.006197	RPL18A; RPL22
GO Biological Process 2021	ncRNA processing (GO:0034470)	2/201	0.001468	0.006197	RPL18A; RPL22
GO Biological Process 2021	ribose phosphate metabolic process (GO:0019693)	1/5	0.001499	0.006197	NUDT5
GO Biological Process 2021	ribosome localization (GO:0033750)	1/5	0.001499	0.006197	EIF6
GO Biological Process 2021	mature ribosome assembly (GO:0042256)	1/5	0.001499	0.006197	EIF6

The enrichment results revealed a clear temporal pattern of PD-1–mediated signaling: early perturbation of immune and coagulation pathways at 5 minutes $\rightarrow$ a transitional state at 20 minutes $\rightarrow$ robust suppression of translation and metabolism at 4 hours. This time-dependent trajectory aligns with the known immunosuppressive role of PD-1.

3.3.2 Cluster Enrichment Analysis

After performing Z-value-based cluster analysis and KEGG pathway enrichment analysis on each cluster, I found that different clusters exhibited different functional patterns.

In Cluster 0, unadjusted results highlighted enrichment in pathways such as Ribosome, Coronavirus disease, and Necroptosis, driven by key genes including RPLP1, RPL22, and PPIA. After FDR correction, Cluster 0 remained strongly enriched in the Ribosome pathway, with additional enrichment in metabolic pathways (e.g., TCA cycle and glyoxylate/dicarboxylate metabolism) as well as the complement and coagulation cascades, involving genes such as RPL18A, RPL22, and CS. These findings suggest that Cluster 0 plays a critical role in translational regulation and metabolic control, with potential links to immune-related processes.

Table 7: Clustering-based functional enrichment analysis results (without FDR adjustment).

Term	Adjusted P-value	Overlap	Genes
Cluster 0 Top 5 KEGG Pathways			
Ribosome	0.006458	2/158	RPLP1; RPL22
Coronavirus disease	0.006857	2/232	RPLP1; RPL22
Necroptosis	0.069330	1/159	PPIA
Cluster 1 Top 5 KEGG Pathways			
No significant pathways detected			

In contrast, Cluster 1 showed no significant enrichment before FDR correction. However, after FDR adjustment, this cluster was enriched in several immune- and

disease-related pathways, including African trypanosomiasis, Malaria, Systemic lupus erythematosus, Necroptosis, and Alcoholism, primarily driven by HBA2 and H2AC21. This indicates that Cluster 1 is more strongly associated with immune responses and inflammation-related processes.

Table 8: Clustering-based functional enrichment analysis results (with FDR adjustment).

Term	Adjusted P-value	Overlap	Genes
Cluster 0 Top 5 KEGG Pathways			
Ribosome	0.018514	2/158	RPL18A; RPL22
Coronavirus disease	0.019705	2/232	RPL18A; RPL22
Glyoxylate and dicarboxylate metabolism	0.032833	1/30	CS
Citrate cycle (TCA cycle)	0.032833	1/30	CS
Complement and coagulation cascades	0.066628	1/85	PLG
Cluster 1 Top 5 KEGG Pathways			
African trypanosomiasis	0.014981	1/37	HBA2
Malaria	0.014981	1/50	HBA2
Systemic lupus erythematosus	0.018811	1/135	H2AC21
Necroptosis	0.018811	1/159	H2AC21
Alcoholism	0.018811	1/186	H2AC21

The modular analysis highlights a functional division of labor among PD-1-associated proteins: Cluster 0 is mainly involved in translation and metabolic regulation, while Cluster 1 is linked to immune and inflammatory pathways. These results further support the notion that PD-1 signaling orchestrates a dynamic regulation of immune suppression and metabolic inhibition across different time points.

3.4 Protein-protein interaction (PPI) network

I used the STRING database (v11.5) to construct a protein-protein interaction (PPI) network. For each time point, the significant proteins (both raw and FDR-adjusted) were submitted to STRING with a minimum interaction score of 0.4. Isolated nodes were retained to ensure the complete presentation of the input protein set.

At the 5-minute time point, the PPI network without FDR adjustment showed several small clusters, including a hemoglobin-related module (HBD, HBG2, HBQ1, HBM, AHSP) and isolated nodes such as CACTIN and HNRNPLL. After FDR correction, the network shifted, highlighting HBA2-centered interactions, including connections with HPX and PLG, suggesting a focus on hemoglobin and coagulation-related pathways.

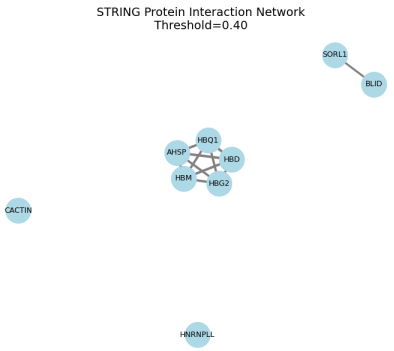

(a) Original protein network.

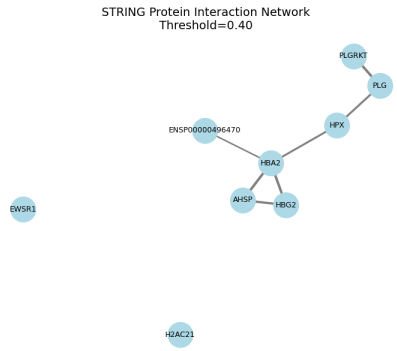

(b) Adjusted protein network.

Figure 4: STRING protein interaction network (5 minutes).

At the 20-minute time point, the raw results produced a network dominated by LNPK-centered interactions, involving MTX2, HOXD1, and EVX2, while other proteins remained isolated. In contrast, the FDR-adjusted network revealed a more ribosomal-centered module, featuring strong interconnections among RPLP1, RPL22, RPL32, and PPIA, pointing toward translation-related regulation.

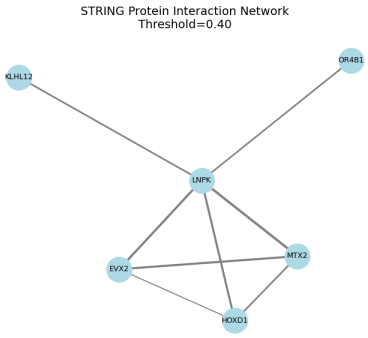

(a) Original protein network.

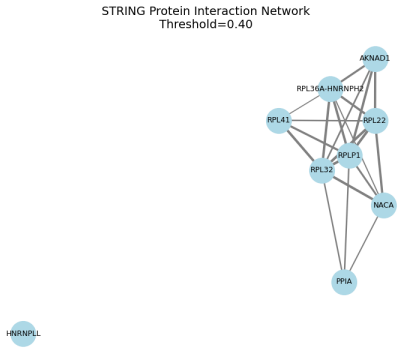

(b) Adjusted protein network.

Figure 5: STRING protein interaction network (20 minutes).

At the 4-hour time point, both raw and FDR-adjusted analyses showed robust ribosomal protein clusters. In the uncorrected results, RPLP1, RPL22, RPL32, and NACA formed a tightly connected module, whereas after FDR correction, additional ribosomal proteins (RPL18A, RPL36, RPL37, EIF6) appeared, reinforcing ribosome-related functional enrichment. Notably, some isolated nodes such as NUDT5 and CS persisted across conditions, indicating unique functional roles outside the main ribosomal modules.

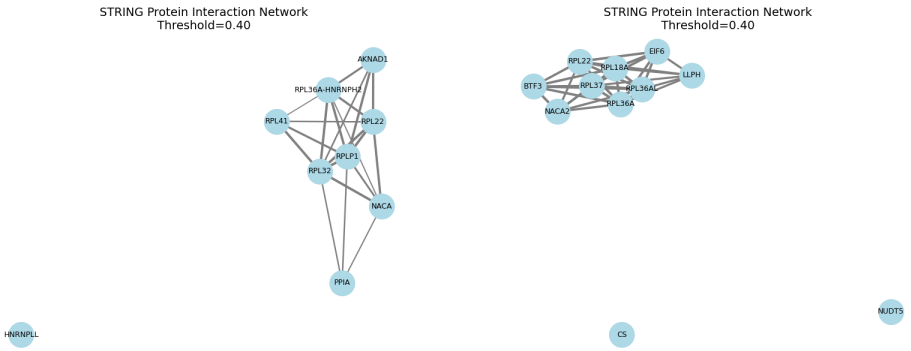

(a) Original protein network.

(b) Adjusted protein network.

Figure 6: STRING protein interaction network (4 hours).

This reflects that PPI analysis revealed changes in the protein interaction network over time following PD-1 activation. Early responses (5 min) were dominated by hemoglobin-associated proteins, while later stages (20 min and 4 h) increasingly converged on ribosomal and translational machinery, suggesting dynamic regulation of cellular processes over time.

3.5 Clustering and Visualization

To further explore the dynamic expression patterns of the most significant proteins, hierarchical clustering and time-series clustering analyses were performed based on standardized protein expression values (Z-scores).

Table 9: Top 30 genes Z-score standardization results (with and without FDR correction).

(a) Without FDR correction.

Gene	5 min	20 min	4 h
HBD	0.1171	0.0533	0.0810
RPLP1	0.0068	0.1338	0.0590
RPL22	0.1750	0.3426	0.2563
PPIA	1.4095	1.5725	1.1935
BLTP3A	1.0158	1.0878	1.0873
H2BC20P	0.5087	0.5219	0.5681
CACTIN	-0.4728	-0.6579	-0.6318
HNRNPLL	-0.1069	-0.1986	-0.0936
SORL1	-0.1175	-2.2597	0.0463
LNPK	-2.5356	-0.5957	-2.5661

(b) With FDR correction.

Gene	5 min	20 min	4 h
CS	-0.4787	-0.5492	-0.6580
PLG	-0.9230	-0.9035	-0.6457
BTF3	-1.2416	-1.1510	-1.0744
RPL22	-0.0271	0.2173	-0.3123
EIF6	-0.0654	-0.2262	-0.1381
HBA2	1.6264	1.7127	1.6342
EWSR1	-0.1411	-0.3308	-0.0366
RPL18A	-0.4070	-0.3551	-0.5148
H2AC21	2.0873	2.0243	2.1803
NUDT5	-0.4299	-0.4386	-0.4346

When using the top 30 differential proteins without FDR correction, two distinct temporal trends were observed: one cluster maintained relatively stable expression

levels across all time points, while the other exhibited marked fluctuations, particularly at 20 minutes (e.g., SORL1 and LNPK showed strong downregulation at this time point). In contrast, after applying FDR correction, the clustering results revealed a clearer separation between expression profiles. For instance, proteins such as HBA2 and H2AC21 consistently showed strong upregulation, whereas proteins including CS, PLG, and BTF3 remained downregulated throughout the time course.

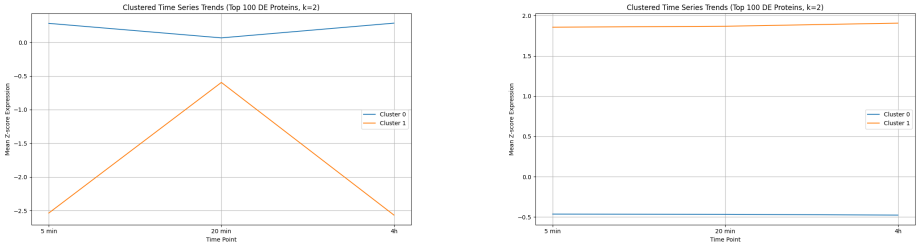

(a) Original clustered time. (b) Adjusted clustered time.

Figure 7: Clustered time teries analysis.

The heatmaps further illustrated these clustering differences, with the FDR-adjusted results highlighting more coherent expression modules.

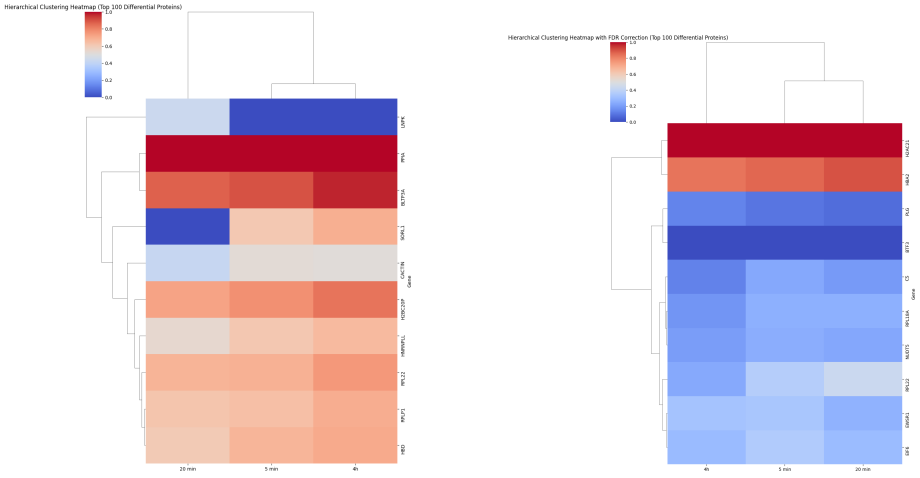

(a) Original clustering heatmap. (b) Adjusted clustering heatmap.

Figure 8: Clustering heatmap.

These findings suggest that FDR correction reduces noise and strengthens the identification of biologically relevant protein clusters, thereby providing a more robust interpretation of the temporal proteomic response.

4 Conclusions

In this project, I systematically profiled the proteomic changes induced by PD-1 activation across multiple time points following TCR stimulation. My analyses revealed that PD-1 signaling exerts time-dependent regulatory effects, with early responses being transient and less stable, while later stages consolidate into more coherent and biologically meaningful proteomic signatures. Differential expression and clustering highlighted both upregulated proteins (e.g., HBA2, H2AC21) and downregulated proteins (e.g., CS, PLG, BTF3), and enrichment analyses linked these clusters to pathways related to ribosomal activity, viral defense, metabolism, and immune regulation. Importantly, applying FDR correction increased the robustness of these findings by reducing false positives and emphasizing biologically relevant modules.

Taken together, my results provide proteomic-level evidence that PD-1 activation reshapes TCR-driven signaling in a temporally dynamic manner, thereby contributing to a deeper understanding of immune checkpoint inhibitor (ICI) mechanisms. By uncovering key proteins and pathways associated with PD-1-mediated regulation, this work also offers potential insights into the processes underlying resistance development and highlights candidates that may serve as novel therapeutic targets.

References

[1] Han, Y., Liu, D., & Li, L. (2020). PD-1/PD-L1 pathway: current researches in cancer. *American Journal of Cancer Research*, *10*(3), 727-742.

[2] Mizuno, R., Sugiura, D., Shimizu, K., Maruhashi, T., Watada, M., Okazaki, I. M., & Okazaki, T. (2019). PD-1 Primarily Targets TCR Signal in the Inhibition of Functional T Cell Activation. *Frontiers in immunology*, *10*, 630. https://doi.org/10.3389/fimmu.2019.00630.

[3] Chen, H. Z., Kim, N. H., Nishizaki, D., Nesline, M. K., Conroy, J. M., DePietro, P., ... & Kurzrock, R. (2025). PD-1 transcriptomic landscape across cancers and implications for immune checkpoint blockade outcome. *NPJ Genomic Medicine*, *10*(1), 21. https://doi.org/10.1038/s41525-025-00465-9.

[4] Hasselmo, M. E., Schnell, E., & Barkai, E. (1995). Dynamics of learning and recall at excitatory recurrent synapses and cholinergic modulation in rat hippocampal region CA3. *Journal of Neuroscience*, *15*(7), 5249-5262.